Fabrication and Analysis of 150-mm-Aperture Nb_3Sn MQXF Coils

E. F. Holik, G. Ambrosio, M. Anerella, R. Bossert, E. Cavanna, D. Cheng, D. R. Dietderich, P. Ferracin, A. K. Ghosh, S. Izquierdo Bermudez, S. Krave, A. Nobrega, J. C. Perez, I. Pong, E. Rochepault, G. L. Sabbi, J. Schmalzle, and M. Yu

***Abstract*—The U.S. LHC Accelerator Research Program (LARP) and CERN are combining efforts for the HiLumi-LHC upgrade to design and fabricate 150-mm-aperture interaction region quadrupoles with a nominal gradient of 130 T/m using Nb_3Sn. To successfully produce the necessary long MQXF triplets, the HiLumi-LHC collaboration is systematically reducing risk and design modification by heavily relying upon the experience gained from the successful 120-mm-aperture LARP HQ program. First-generation MQXF short (MQXFS) coils were predominately a scaling up of the HQ quadrupole design, allowing comparable cable expansion during Nb_3Sn formation heat treatment and increased insulation fraction for electrical robustness. A total of 13 first-generation MQXFS coils were fabricated between LARP and CERN. Systematic differences in coil size, coil alignment symmetry, and coil length contraction during heat treatment are observed and likely due to slight variances in tooling and insulation/cable systems. Analysis of coil cross sections indicate that field-shaping wedges and adjacent coil turns are systematically displaced from the nominal location and the cable is expanding less than nominally designed. A second-generation MQXF coil design seeks to correct the expansion and displacement discrepancies by increasing insulation and adding adjustable shims at the coil pole and midplanes to correct allowed magnetic field harmonics.**

***Index Terms*—High-luminosity LHC, low-beta quadrupole, Nb_3Sn magnet, superconducting accelerator magnets.**

I. Introduction

SUPERCONDUCTING accelerator magnets traditionally used NbTi as the sole workhorse conductor until now. The High Luminosity LHC upgrade requires Nb_3Sn technology to obtain the necessary dipole field to free-up space and necessary inner triplet gradient and aperture to sufficiently decrease the interaction point beam size [1]. The US LHC Accelerator Research Program or LARP has developed Nb_3Sn technology in quadrupole magnets starting from the 90 mm aperture Technology Quadrupole (TQ) and the 4.5 m magnetic length Long TQ [2], and moving toward the 120 mm aperture HQ and LHQ coils [3], [4]. LARP constructed a total of 26 HQ coils with multiple successful full magnet tests [5]–[8] and is the baseline design for the joint CERN/LARP development of the 150 mm MQXF IR quadrupoles [9], [10]. MQXF will operate at 16.5 kA with a peak field and gradient of 11.4 T and 132.6 T/m. MQXFA magnets have a 4.2 m magnetic length and will be fabricated by LARP while MQXFB magnets have a 7.15 m magnetic length and will be fabricated by CERN. To date a total of 13 coils of 1.5 m magnetic length were fabricated between CERN and LARP. One coil in mirror configuration tested to 91% short sample [11]. Only two of the fabricated coils had minor flaws: swapped end parts and weak splice. All coils fabricated were electrically sound with no electrical shorts.

Manuscript received October 19, 2015; accepted December 31, 2015. Date of publication January 12, 2016; date of current version January 27, 2016. The work of E. F. Holik was supported by the Toohig Fellowship in Accelerator Science from the US LHC Accelerator Research Program. This work was supported in part by the Office of High Energy and Nuclear Physics, U.S. Department of Energy, under Contract Lawrence Berkeley National Laboratory DE-AC02-05CH11231; by the Fermi National Laboratory DE-AC02-07CH11259; by the Brookhaven National Laboratory DEAC02-98CH10886; and by the European Commission under the FP7 project HiLumi LHC under Grant GA 284404.

E. F. Holik, G. Ambrosio, R. Bossert, S. Krave, A. Nobrega, and M. Yu are with the Fermi National Accelerator Laboratory, Batavia, IL 60510 USA (e-mail: eholik@fnal.gov).

M. Anerella, A. K. Ghosh, and J. Schmalzle are with the Brookhaven National Laboratory, Upton, NY 11973 USA.

E. Cavanna, P. Ferracin, S. Izquierdo Bermudez, J. C. Perez, and E. Rochepault are with the European Organization for Nuclear Research (CERN), 1211 Geneva, Switzerland.

D. Cheng, D. R. Dietderich, I. Pong, and G. L. Sabbi are with the Lawrence Berkeley National Laboratory, Berkley, CA 94720 USA.

Color versions of one or more of the figures in this paper are available online at http://ieeexplore.ieee.org.

Digital Object Identifier 10.1109/TASC.2015.2514193

II. MQXF 1st Generation Coil Features

A. Nb_3Sn Rutherford Cable

MQXF Rutherford cable is comprised of 40 strands of 0.85 mm diameter wire. Restacked Rod Process conductor by Oxford Superconducting Technologies was used for the majority of the coils with two coils fabricated by Powder-in-Tube conductor from Bruker-EAS [12]. All LARP conductor is cabled at Lawrence Berkeley National Lab. The cable includes a 25 μm thick by 10–12 mm wide stainless steel core for reducing inter-strand coupling currents [13]. The cable is insulated by directly braiding on two plies of 66 TEX S2 Glass filaments with a target thickness of 145 ± 5 μm at 5 MPa as seen on the cable in Fig. 1. CERN insulation measured 146 ± 3 μm while LARP insulation measured 143 ± 3 μm.

B. Coil Winding and Curing

Nb_3Sn conductor is brittle in nature and requires a wind-and-react technique so that the actual superconductor is formed when the cable is in final shape. The Rutherford cable is wound around a segmented Ti-6Al-4V pole with an alignment keyway feature to aid in assembling the coils into a magnet structure as seen in the top groove in Fig. 2 [14]. The titanium alloy contracts less than the surrounding materials at cryogenic

Fig. 1. Picture of "accordion style" end parts first employed in LHQ. The end parts are plasma coated with alumina at 250-μm thickness for additional electrical integrity. The added flexibility accommodates the tendency for cable to separate from the winding mandrel surface also called cable spring-back. The inner end part tightly conforms to cable shape and the outer end part will easily conform to the inner turns after the addition of subsequent tooling and turns.

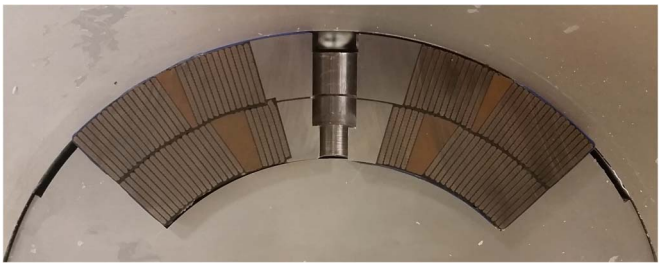

Fig. 2. Picture of MQXFS practice coil 1 within impregnation form block (top coil) and mandrel block (bottom coil). The beginning of the inner layer to outer layer transition can be seen on the left side of the pole. The coil outer diameter and top keyway groove align each coil during magnet assembly of four coils. The coil innermost and outermost radii are 74.75 and 113.376 mm, respectively.

temperatures applying additional preload to the pole turns. Gaps are placed between pole segments to allow for cable contraction during heat treatment [15]. A ceramic binder (CTD-1202X) is used while winding that acts as a bonding agent to reduce popped strands at the coil ends. CERN uses a winding tool for the same effect. The same binder is applied over the entire coil after winding and cured at 120 °C for ease of handling and to enable transfer to reaction tooling after winding [16]. All LARP QXF coils to date were wound and cured at FNAL.

C. Coil Reaction and Impregnation

After winding and curing the coil must undergo a Nb_3Sn formation heat treatment. Typical heat treatments are for one week with a peak temperature of 640 °C for 48 hours. Directly after reaction, NbTi cables are spliced to the newly embrittled Nb_3Sn leads for support. Electrical wiring and quench protection heaters that would not survive the high temperature heat treatment are then installed onto both the coil outer and inner diameters. Afterward the coil is vacuum pressure impregnated with CTD-101K epoxy to support individual strands and is acceptable for the radiation dose expected for Hi-Lumi IR quads [17], [18].

III. Fabricated Coil Size and Symmetry

Uniform pre-load and field homogeneity require precise coil positioning and alignment during magnet assembly [14], [19], and [20]. Size variances along the coil length and between coils likely create non-uniform loading and non-uniform magnetic fields. Keyway, coil outer diameter, and midplane surfaces are all measured by a Coordinate Measurement Machine (CMM) to quantify these variances.

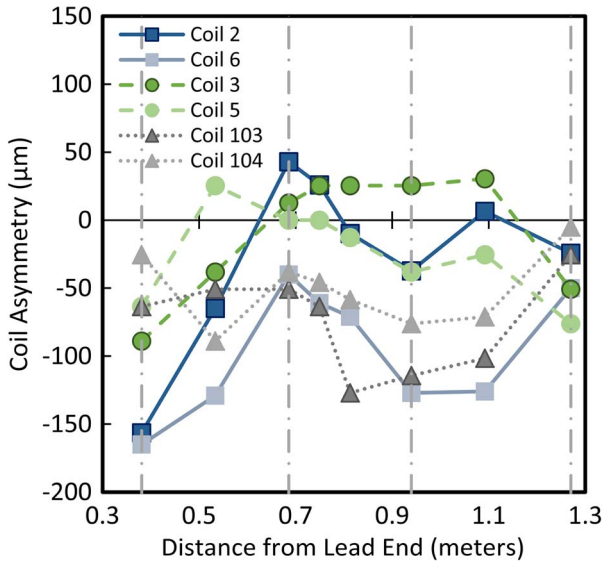

Fig. 3. Coil symmetry defined as the amount the transition side midplane is larger than the right midplane based on a coil outer diameter and keyway CMM best fit. The vertical dashed lines indicate pole alignment pin locations. FNAL reacted and impregnated coils 2 and 6. BNL and CERN reacted coils 3, 5 and 103, 104, respectively. Coils reacted and impregnated with the same tooling differ by 55 μm RMS, a value less than tooling clearances might suggest. The RMS range for all coils is much larger approaching 130 μm.

All reaction and impregnation tooling is quality checked to maintain tight control on the overall coil size. The tooling surface tolerance of the actual outer and inner diameters and coil midplanes is 50 μm. Reaction and impregnation tooling includes periodic alignment pins to center the pole relative to the coil midplanes. Original tolerance buildup on the alignment pins allow slightly more variation (175 μm) and is reflected by the coil asymmetry variation between coil made with different tooling sets as shown in Fig. 3.

A. Impregnated Coil Asymmetry

The CMM maps transverse coil outlines at multiple locations along the coil length. The coil outer diameter and pole keyway align and position each coil in the magnet collar and flux return structure [14]. Therefore, the CMM 'best fits' the coil outer diameter and pole keyway to the nominal coil geometry. Midplane surfaces are then measured for deviations from nominal. The left midplane as viewed from the coil lead end is the same side as the layer 1 to layer 2 transitional jump. Coil asymmetry is then defined as the amount that the left or transition midplane is larger than the right midplane.

1) Asymmetry Trends: Asymmetry variation between coils from one tooling source is only 55 μm whereas coils fabricated by different tooling sets vary by 130 μm. This strongly suggests that the asymmetry is being driven by the reaction and impregnation tooling rather than random variations. Additionally, across all tooling sets there seems to be a slight negative bias

in asymmetry implying that the coil transition side is slightly larger than the non-transition side by 50 μm. This is equivalent to shifting midplanes in a magnet 2D cross section. The normal (b_n) and skew (a_n) components of the field harmonics are defined as

$$B_y + iB_x = 10^{-4} \sum (b_n + ia_n) \left(\frac{x+iy}{R_{\text{ref}}} \right)^{n-1} \quad (1)$$

where B_x and B_y are the components of the magnetic field, B_2 is the main quadrupole component and R_{ref} is the reference radius, which is 2/3 of the aperture or 50 mm. A single midplane shift of 50 μm due to coil variation along the length produces a full unit of a_3 and half a unit of a_4 using (1). One unit of a_6 is produced if all midplanes are systematically shifted by 50 μm. In short, the asymmetry and variation is likely to drive roughly one unit of skew a_3 and a_6.

2) Correcting Coil Asymmetry: Efforts are currently underway to determine which fabrication procedures or tooling is driving the coil asymmetry. A tool was designed and fabricated to measure the coil asymmetry during fabrication. Preliminary results indicate that the reaction and impregnation tooling is driving the asymmetry.

LARP is pursuing two tactics to correct asymmetric coils. The first is to create a slight interference fit between mandrel blocks and form blocks as shown in Fig. 2. Tighter fit is accomplished by placing symmetric shims along the sides of the mandrel block at the form block contact point and should eliminate any small relative motion between the two blocks.

Roughly 1/10th of the outer diameter form blocks are modified to have additional features to align the pole keyway with the tooling or coil center. The second notion is to fabricate additional modified form blocks and only use the blocks that fall within an extremely tight tolerance (± 15 μm). Unused alignment pin form blocks will then simply be used as an ordinary form blocks without alignment pins. These changes are planned for second generation QXF coils.

B. Impregnated Coil Size

Two fabrication features principally drive the final coil size. The primary driver is the specific reaction and impregnation tooling dimension and tolerance as previously discussed. The secondary feature is the cable expansion relative to the coil cavity size.

Cable in HQ01 coils were not allowed to transversely expand and were oversize by 340 μm in the radial and 140 μm in the azimuthal directions on average as presented in Table I. HQ02 cavity size was increased and the average coil size was much closer to nominal. HQ03 tooling allowed less expansion but had even smaller coils on average, indicating that the braided on insulation may constrict the cable growth and ultimately the average coil size.

IV. Cable Insulation and Expansion

Rutherford type Nb_3Sn cable typically expands in width and thickness and contracts in length [21]. Purely from thermal expansion, Rutherford cable expands roughly 6 times that of the ceramic S-2 glass filaments from room temperature to formation temperature [22], [23]. Rutherford cable also chemically expands between 3 and 6 percent volumetrically when Nb and Sn combine to form Nb_3Sn. The total differential in expansion places the S2 Glass insulation filaments in tension and places pressure on the cable.

TABLE I
Allowed Cable Growth and Coil Size

Parameter	HQ01	HQ02	HQ03	MQXF LARP	MQXF CERN
Azimuthal Allowed Growth†	0%	6.0%	3.9%	4.5%	4.5%
Radial Allowed Growth†	0%	1.6%	1.4%	2.0%	2.0%
Cable Insulation Type	Sock	Sock	Braid	Braid‡	Braid‡
Avg. Radial Coil Oversize*	340 μm	120 μm	25 μm	20 μm	-40 μm
Avg. Azimuthal Coil Oversize*	140 μm	75 μm	~0 μm	50 μm	-75 μm
Avg. HT Coil Gap Closure§	<0.01%	0.21%	0.02%	0.16%	0.03%

†The reaction and impregnation tooling are equivalent for all HQ coils. Allowed Growth is calculated based on coil cavity and unreacted cable size.

‡Insulation thicknesses and materials are equivalent but applied with different parameters.

*Coil Oversize is based on overall cross section CMM best fit.

§Avg. HT Coil Gap Closure is the amount the pole gap closed during heat treatment based on pole length [15].

TABLE II
Key Braided-on Insulation Parameters

Parameter	HQ braid	MQXF LARP	MQXF CERN	units
# Carriers	48	48	32	-
Picks per inch *(P/I)*	28.2	18.3	21.6	-
Pitch Length (*PL*)	21.7	33.4	18.8	mm
Pitch angle (*PA*)	56.2°	49.7°	64.4°	-
Strand Length per *PL*	39.0	51.6	43.6	mm
Insulation thickness	0.104	0.143	0.146	mm
Width of Cable (*W*)	14.8	18.15	18.15	mm
Mid-thickness of Cable (*T*)	1.375	1.525	1.525	mm
# Plies / Strand	1	2	2	-

A basket weave of AGY S-2 Glass fibers of 66 TEX with 933 high-temperature silane sizing was used for each type of insulation.

A. Braided-on Insulation and Cable Pressure

Target insulation thickness is 145 μm for first generation MQXF. The number of carriers is not easily adjustable to obtain the target insulation thickness. Only the number of picks per inch and plies per strand remain adjustable to achieve this target thickness. Number of picks per inch determines the pitch angle and pitch length shown in Table II and Fig. 4.

1) Applied Pressure: The pressure applied to the cable from insulation can be calculated from the following geometric equations:

$$\text{Axial } P = \frac{\#\,\text{Carriers}}{W * T} \cos(PA) * \text{Tension} \quad (2)$$

$$\text{Transverse } P = \frac{\#\,\text{Carriers} * 2}{PL * T} \sin(PA) * \text{Tension}. \quad (3)$$

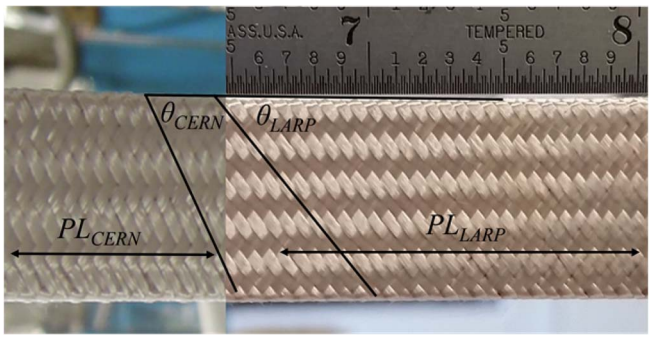

Fig. 4. Two types of braided-on insulation for MQXF. The pitch length and the pitch angle are indicated. The insulation thicknesses are equivalent. The fiducial is in inches.

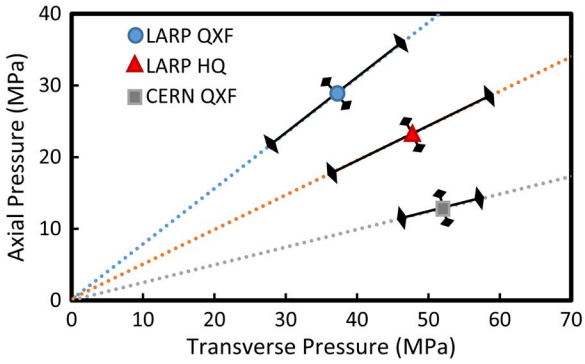

Fig. 5. Theoretical pressure applied to cable from braided on insulation due to cable expansion. The pressures assume no degradation to the insulation due to heat treatment or binder. The uncertainties are due to the range of measured cable expansion values for braided-on insulation from Table III and variances in P/I along the length of the insulated cable.

In (2) and (3), the pressure is calculated from the total insulation tension applied over the cross sectional area of the cable. A factor of 2 is added to the transverse pressure because the insulation wraps over the edge doubling the pressure. Only the insulation tension varies during cable expansion for (2) and (3). The ratio of axial pressure to transverse pressure is the strongest indication of how the insulation constricts cable growth and is given below:

$$\text{Slope} = \frac{(\#\,\text{Carriers})^2}{16 * P/I * W * (W+T)}. \tag{4}$$

The slope from equation (4) defines the slope for each cable insulation system in Fig. 5. The ratio between axial to transverse pressure is dependent upon the square of the number of carriers. For fewer carriers the insulation will preferentially constrict cable width.

2) Insulation Tension: To calculate the tension in the filaments we need to first determine how the cable expansion values in Table III cause the filaments to elongate. The tension is simply due to the strain induced on each strand. The tension for each filament is calculated from the following formula:

$$\text{Tension} = T_0 + \frac{L - L_0}{L_0} E_{S2\ \text{Glass}} A_{S2\ \text{Glass}} \tag{5}$$

where

$$A_{S2\ \text{Glass}} = \text{TEX} * \#\,\text{plies} * \rho_{S2\ \text{Glass}}. \tag{6}$$

TABLE III
MEASURED RUTHERFORD CABLE EXPANSION FROM HEAT TREATMENT

PARAMETER		Free HQ	Braid HQ	Free MQXF	LARP MQXF	CERN MQXF
Width Growth	Max	2.0%†	0.5%†	1.4%‡	0.45%†	0.29%†
	Min	1.6%†	0.2%†	1.0%‡	0.06%‡	0.14%†
Thickness Growth	Max	4.5%‡	5.4%†	3.0%‡	3.4%†	3.0%§
	Min	3.1%‡	3.4%†	2.5%‡	2.9%‡	2.5%§
Length Contraction	Max	0.25%‡	0.14%*	0.55%‡	0.19%*	0.08%*
	Min	0.05%*	0.00%*	0.39%‡	0.01%‡	0.00%*
Transverse Pressure (MPa)	Max	0	59	0	46	57
	Min	0	36	0	28	46

LARP and CERN both use a braided on insulation. Free simply means that the cable is free to expand without any constraint by tooling or insulation.
†Measured expansion from coil cross section analysis [25], [26].
‡Measured expansion from LBNL cable experiments [27].
*Measured contraction from pole gap closure during heat treatment.
§Measured expansion from Cable 10-stacks or direct measurement.

For MQXF the filaments are 66 TEX or 66 grams per 1000 m and there are 2 plies per strand. $E_{S2\ \text{Glass}} = 88$ to 94 GPa and $\rho_{S2\ \text{Glass}} = 2.46$ g/cc is the elastic modulus and density of S2 Glass [22]. For S2 glass the strength and density change very little between room temperature and 650 °C. T_0 is determined by initial carrier tension and is < 5% of the total tension. The unexpanded length of each strand is given by

$$L_0 = \sqrt{PL^2 + (2W + 2T)^2} \tag{7}$$

and the expanded length is given by

$$L = \frac{W}{W+T}\sqrt{((1+\delta_L)PL)^2 + ((1+\delta_W)(2W+2T))^2} + \frac{T}{W+T}\sqrt{((1+\delta_L)PL)^2 + ((1+\delta_T)(2W+2T))^2} \tag{8}$$

where δ is the expansion parameter for length, width, and thickness expressed as a percentage in Table III. The calculated axial and transverse pressures due to the LARP, CERN, and HQ braided on insulations are presented in Fig. 5.

Equations (5) and (6) do not take into account how the insulation weakens during heat treatment. At elevated temperatures a large fraction of the silane sizing is lost and the filament abrasiveness increases and weakens the insulation [27]. Ceramic matrix binder, CTD-1202X, likely increases filament friction after heat treatment and decreases the insulation robustness. The precise effects are unknown but are currently being investigated. The pressures should therefore be interpreted as relative pressures. A 50% decrease in insulation integrity would equate to a 50% decrease in both axial and transverse pressure etc.

B. Cable Expansion

Unconfined MQXF cable expands in width by 1.06% during heat treatment from LBNL cable experiments [26]. The transverse pressure applied by the insulation decreases the width or radial expansion of LARP cable to 0.4% and CERN cable to 0.14%. The growth decrease is consistent with the transverse pressure difference between CERN and LARP. First generation MQXF coil design allowed 2% width growth which equates to a radial free space of 300 μm and 340 μm for LARP and CERN.

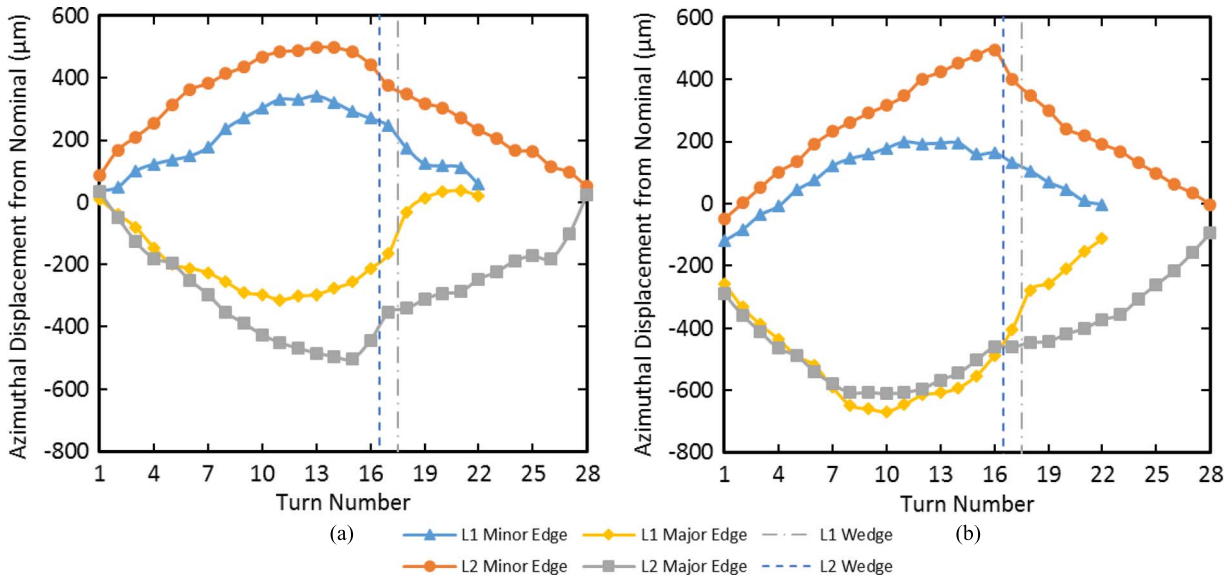

Fig. 6. Azimuthal turn displacements with respect to the designed turn location. (a) and (b) Azimuthal displacements for LARP coil 1 and CERN coil 101. L1 and L2 represent the inner and outer coil layers, and Minor/Major indicate the cable edge displaced. Azimuthally toward the coil midplane is considered a positive shift. Turn 1 is the midplane turn. The average displacements between the transition and nontransition sides of full coil cross section are presented.

In the azimuthal or thickness direction the unconfined MQXF cable expands between 2.5% and 3.1% during heat treatment. Both CERN and LARP cable expand by similar amounts indicating that the cable thickness is largely unaffected by the braided on insulation. This result is not surprising since the insulation will only effect thickness near the cable edges. In other words the high cable aspect ratio allows the cable to expand without constriction in the azimuthal direction up to the cavity size of 5.2% for first generation. The cavity size comes from the designed growth of 4.5% and the cable insulation measuring 5 μm smaller than designed.

C. MQXF Pole Gaps

During winding, gaps are placed along the pole to allow the coil to contract from the winding tension and from conductor contraction during heat treatment [15]. Unconfined cable expands in width allowing the length to contract. The braided on insulation applies a transverse pressure that constricts width growth thus reducing the length contraction.

Pole gap closure during heat treatment for MQXF coils is very consistent with the cable contraction from experiments. Unconfined cable contracted 0.45% on average. LARP Expansion experiments with braided on insulation contracted 0.09% while the pole gaps closed 0.14% [26]. The small 0.05% discrepancy is likely caused by end effects or the welds from the expansion experiments [21]. CERN pole gaps closed on average 0.03% consistent with higher transverse pressure. Insulation or friction during heat treatment may also be causing different pole gap closures and is currently being investigated [28].

V. Coil Cross Section Analysis

Multiple techniques are available to analyze coil cross sections. The most efficient approach is to create a high-contrast image or scan of each cross section and process the image with cable locating subroutines. This approach is limited by the accuracy of the image but is not limited by manual cable edge defining and associated uncertainties. A less efficient method includes using an optical comparator or CMM to manually plot each cable edge. This process is slow but is not subject to scaling uncertainties. A cross section of LARP coil 1 was analyzed with an optical comparator and a cross section of CERN coil 101 was analyzed with image post processing [24], [25].

A. Azimuthal Turn Displacement

Azimuthal displacements are presented in Fig. 6(a) and (b). The displacements are unexpectedly large but are very similar between LARP coil 1 and CERN coil 101. For L2 the maximum difference in displacement between the minor and major edge is at the same turn and has the same magnitude for both coils (turn 14 and 995 μm). This is consistent with the with the L2 azimuthal free space of 880 μm as calculated from the difference in coil cavity size and cable thickness expansion measurements.

Maximum difference in L1 azimuthal displacements also occurs at the same location for both coils but with different magnitudes (turn 11 and 645 μm for coil 1 and 845 μm for coil 101). These values are again consistent with the L1 azimuthal free space of 690 μm. Both peak displacements for both layers and both coils occur at the central turn; there are 28 turns in L2 and 22 turns in L1.

Despite substantial azimuthal displacement, plots for both coils have remarkably similar shape with the minor edge shifting toward the midplane and the major edge shifting toward the pole. During fabrication the cable tends to spring-back into the traditional flat or pancake shape near the coil ends rotating the minor edge away from the pole and the major edge toward the pole. Therefore it is hoped that this tendency will reduce in MQXF long coils.

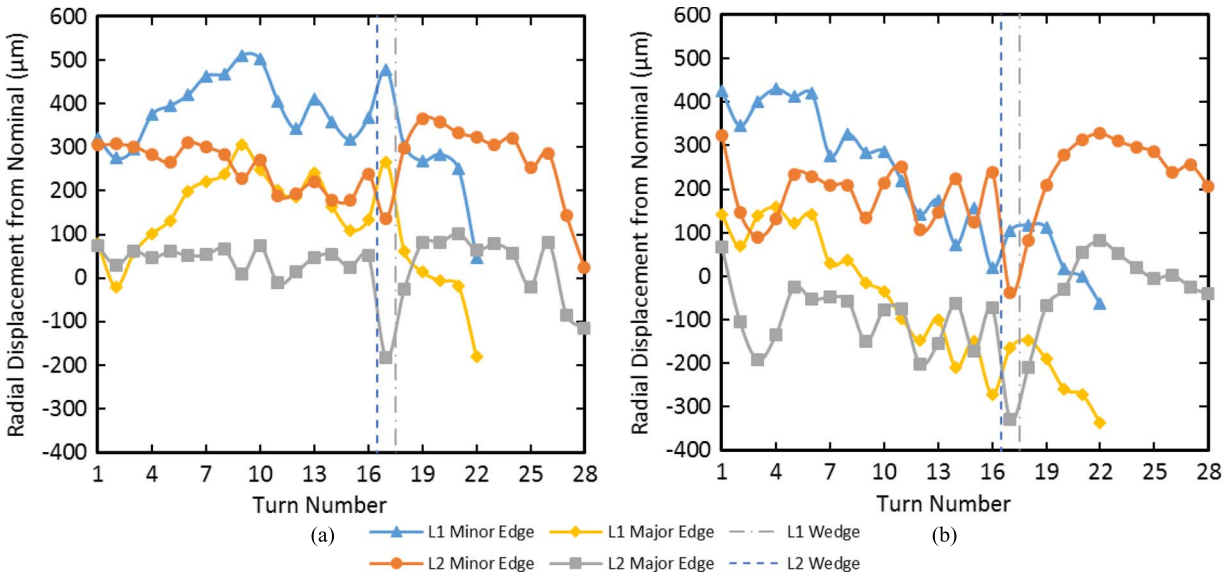

Fig. 7. Radial turn displacements with respect to the designed turn location. (a) and (b) Radial displacements for LARP coil 1 and CERN coil 101. L1 and L2 represent the inner and outer coil layers. Radially outward is considered a positive shift. Turn 1 is the midplane turn. The average displacement between the transition and nontransition sides of a full coil cross section is presented. The minor and major edges of each layer track well. The difference between the minor and major edges is due to the less-than-expected width growth with respect to nominal.

B. Radial Turn Displacement

The total radial free space is 600 μm for LARP and 680 μm for CERN as calculated from cavity size and different measured width expansions. The spring-back effect and free space would suggest that the L2 major edge would be minimally displaced while the L1 minor edge would be maximally displaced. This general trend is seen in the radial displacements presented in Fig. 7(a) and (b). The peak radial displacement is 510 μm for LARP and 430 μm for CERN both occurring along the L1 minor edge. Large inward shifts occur at turns adjacent to the wedge due to the rotation of the wedge as indicated in the azimuthal displacement figures. Large inward displacements also occur near the L1 pole indicating that the interlayer insulation and L2 pole is overly pressing the pole turns inward.

VI. Second Generation MQXF

Second generation MQXF incorporates several small adjustments to the coil design with the goal of reducing risk [12]. The cable keystone was reduced from 0.55° to 0.4° to reduce the plastic deformation to the cable minor edge. Extra insulation at the midplane and the pole will also enable adjustment to the b_6 harmonic by azimuthally shifting all coil blocks during fabrication in second generation MQXF [12]. The assumed width growth was reduced from 2.0% to 1.2% taking up better than half of the discrepancy between assumed and measured width expansion during heat treatment. Designed insulation thickness was reduced from 150 μm to 145 μm representing insulation measurements [12]. All S2 Glass insulation is qualified by measurement at 5 MPa rather than accepting the generally oversized nominal manufacturer thickness. More extensive reductions to assumed growth increase the risk of electrical shorts during heat treatment and reduced quench performance [5], [29].

VII. Conclusion

MQXF has benefited tremendously from the HQ coil development with arguably the highest 'out of the gate' success rate for a new Nb_3Sn coil design. Coil asymmetries may drive non-uniform loading and undesirable harmonics, but slight modifications to tooling should reduce the asymmetries. Turn displacements are consistent with the designed free space and will be reduced while maintaining electrical and quench protection integrity in second generation QXF coils.

Braided on S2 Glass insulation constricts cable width growth and length contraction. This observation will help fine tune fabrication parameters moving toward second generation MQXF. For future Nb_3Sn coils, insulation parameter adjustments could sufficiently reduce width expansion and length contraction to enabling longer coil fabrication lengths and tighter constraints on turn location.

The first magnet assembly was recently completed with combined CERN and LARP coils. The test will soon be completed with high hopes toward the full development of Hi-Lumi MQXF magnets.

References

[1] E. Todesco *et al.*, "Design studies for the low-beta quadrupoles for the LHC luminosity upgrade," *IEEE Trans. Appl. Supercond.*, vol. 23, no. 3, Jun. 2013, Art. ID 4003305.

[2] G. Ambrosio *et al.*, "Design of Nb_3Sn coils for LARP long magnets," *IEEE Trans. Appl. Supercond.*, vol. 17, no. 2, pp. 1035–1038, Jun. 2007.

[3] H. Felice *et al.*, "Design of HQ—A high field large bore Nb_3Sn quadrupole magnet for LARP," *IEEE Trans. Appl. Supercond.*, vol. 19, no. 3, pp. 1235–1239, Jun. 2009.

[4] G. L. Sabbi, "Progress in high field accelerator magnet development by the US LHC accelerator research program," EuCARD-AccNet-EuroLumi Workshop, Malta, CERN, Geneva, Switzerland, Yellow Rep. CERN-2011-003, 2011, pp. 30–36.

[5] S. Caspi *et al.*, "Results of 15 T Nb_3Sn quadrupole magnet HQ01 with a 120 mm bore for the LHC luminosity upgrade," *IEEE Trans. Appl. Supercond.*, vol. 21, no. 3, pp.1854–1857, Jun. 2011.

[6] G. Chlachidze *et al.*, "Performance of HQ02, an optimized version of the 120 mm Nb_3Sn LARP quadrupole," *IEEE Trans. Appl. Supercond.*, vol. 24, no. 3, pp. 1–5, Jun. 2014.

[7] H. Bajas *et al.*, "Test results of the LARP HQ02b magnet at 1.9 K," *IEEE Trans. Appl. Supercond.*, vol. 24, no. 3, pp.1–5, Jun. 2014.

[8] J. DiMarco *et al.*, "Magnetic field measurement and correction in the LARP HQ03 Nb_3Sn quadrupole," *IEEE Trans. Appl. Supercond.*, to be published.

[9] E. Todesco *et al.*, "A first baseline for the magnets in the high luminosity LHC insertion regions," *IEEE Trans. Appl. Supercond.*, vol. 24, no. 3, Jun. 2014, Art. ID 4002405.

[10] G. Ambrosio, "Nb_3Sn high field magnets for the high luminosity LHC upgrade project," *IEEE Trans. Appl. Supercond*, vol. 25, no. 3, Jun. 2015, Art. ID 4002107.

[11] G. Ambrosio *et al.*, "Test results of the first short coil and of the first short model for the LHC inner triplet upgrade," presented at the 24th Magnet Technol. Conf., Seoul, Korea, Oct. 18–23, 2015.

[12] S. Izquierdo Bermudez *et al.*, "Second-generation coil design of the Nb_3Sn low-ß Quadrupole for the High Luminosity LHC," *IEEE Trans. Appl. Supercond.*, to be published.

[13] X. Wang *et al.*, "Multipoles induced by inter-strand coupling currents in LARP Nb_3Sn quadrupoles," *IEEE Trans. Appl. Supercond.*, vol. 24, no. 3, Jun. 2014, Art. ID 4002607.

[14] P. Ferracin *et al.*, "Magnet design of the 150 mm aperture low-ß quadrupoles for the high luminosity LHC," *IEEE Trans. Appl. Supercond.*, vol. 24, no. 3, pp.1–6, Jun. 2014.

[15] F. Borgnolutti *et al.*, "Fabrication of a third generation of Nb_3Sn coils for the LARP HQ03 quadrupole magnet," *IEEE Trans. Appl. Supercond.*, vol. 24, no. 3, Jun. 2014, Art. ID 4002505.

[16] F. Borgnolutti *et al.*, "Fabrication of a second-generation of Nb_3Sn coils for the LARP HQ02 quadrupole magnet," *IEEE Trans. Appl. Supercond.*, vol. 24, no. 3, Jun. 2014, Art. ID 4003005.

[17] J. Polinski *et al.*, "Certification of the radiation resistance of coil insulation material," EuCARD Deliverable Report, Eur. Coordination Accel. Res. Develop., Geneva, Switzerland, EuCARD-Del-D7-2-1-final-1.docx.

[18] R. Bosser *et al.*, "Recent progress and tests of radiation resistant impregnation materials for Nb_3Sn coils," in *Proc. AIP Conf.*, Jun. 2014, vol. 1574, pp.132–139.

[19] S. Caspi *et al.*, "Design of a 120 mm bore 15 T quadrupole for the LHC upgrade phase II," *IEEE Trans. Appl. Supercond.*, vol. 20, no. 3, pp. 144–147, Jun. 2010.

[20] P. Ferracin *et al.*, "Azimuthal coil size and field quality in the main CERN Large Hadron Collider dipoles," *Phys. Rev. Spec. Topics—Accel. Beams*, vol. 5, 2002, Art. ID 062401.

[21] D. Bocian, G. Ambrosio, and G. M. Whitson, "Measurements of Nb_3Sn conductor dimension changes during heat treatment," in *Proc. AIP Conf.*, Jun. 2011, vol. 1435, pp. 193–200.

[22] D. R. Dietderich, J. R. Litty, and R. M.Scanlan, "Dimensional changes of Nb_3Sn, Nb_3Al and $Bi_2Sr_2CaCu_2O_8$ conductors during heat treatment and their implication for coil design," *Adv. Cryogenic Eng.*, vol. 44B, pp. 1013–1320, Jun. 1998.

[23] Technical Paper, AGY, Aiken, SC, USA, Pub. No. LIT-2006-11 R2, Feb. 2006, [Accessed on Oct. 11, 2015]. [Online]. Available: http://www.agy.com/wp-content/uploads/2014/03/High_Strength_Glass_Fibers-Technical.pdf

[24] E. Rochepault *et al.*, "Dimensional changes of Nb_3Sn Rutherford cables during heat treatment," *IEEE Trans. Appl. Supercond.*, to be published.

[25] I. Pong, D. R. Dietderich, A. Ghosh, and E. F. Holik, "Different methods for studying and analyzing dimensional change due to heat treatment of Nb_3Sn Rutherford cable for accelerator magnets coils," presented at the 12th Eur. Conf. Appl. Supercond., Lyon, France, Sep. 6, 2015, 2A-LS-P-02.11.

[26] I. Pong, D. R. Dietderich, and A. Ghosh, "Dimensional changes of Nb_3Sn cables during heat treatment," presented at the Int. Cryogenic Mater. Conf., Tucson, AZ, USA, Jun. 28, 2015, C2OrF.

[27] H. M. Yun and J. A. DiCarlo, "Thermomechanical characterization of SiC Fiber Tows and Implications for CMC," in *Proc. 12th Int. Conf. Composite Mater.*, Paris, France, Jul. 5–9, 1999, Paper 594.

[28] M. Durante *et al.*, "Nb_3Sn Rutherford cables geometrical behavior during heat treatment," *IEEE Trans. Appl. Supercond.*, to be published.

[29] H. Felice *et al.*, "Impact of coil compaction on Nb_3Sn LARP HQ magnet," *IEEE Trans. Appl. Supercond.*, vol. 22, no. 3, Jun. 2012, Art. ID 4001904.